Thermochimica Acta 694 (2020) 178797

Contents lists available at ScienceDirect

Thermochimica Acta

journal homepage: www.elsevier.com/locate/tca

Kinetic study of the thermo-oxidative decomposition of metformin by isoconversional and theoretical methods

Ismail Badran [a], Abdallah D. Manasrah [b], Azfar Hassan [b], Nashaat N. Nassar [b,*]

[a] Department of Chemistry and Earth Sciences, Qatar University, P.O. Box: 2713, Doha, Qatar
[b] Department of Chemical and Petroleum Engineering, University of Calgary, 2500 University Street NW, Calgary, Alberta, T2N 1N4, Canada

ARTICLE INFO

Keywords:
Metformin
Isoconversional method
Oxidation
DFT
Reaction mechanism

ABSTRACT

The drug metformin is the most prescribed drug to treat type II diabetes and has been recently reported to have anticancer activities. Because of its wide use, its potential risk on the environment is extremely concerning. In this study, the mechanism and the thermodynamics of the thermo-oxidative decomposition of the metformin were investigated as part of a new solution for the pharmaceutical contamination of water bodies. Thermogravimetry and mass spectrometry were used to demonstrate the metformin thermo-oxidative decomposition under air in the temperature range 25–800 °C. The isoconversional methods of Kissinger-Akahira Sunose (KAS) and Friedman (FR) were implemented to deduce the trends of effective activation energies. As expected, the effective activation energy (E_α) of the reaction was dependent on the reaction temperature, suggesting multi-step reactions. The E_α ranged from 100 to 145 kJ/mol and 200–300 kJ/mol for the KAS and FR methods, respectively. The kinetic triplet, A_α, $\Delta S^\ddagger$, and $\Delta G^\ddagger$ were also determined by finding the appropriate reaction model. Theoretical calculations were implemented to propose a full reaction mechanism. The oxidation of metformin was investigated with both molecular O_2(t) and atomic O(t) oxygen. The experimental results were then explained under the light of the computational data to explain the variation of E_α with temperature, and the competition between the O_2(t)/O(t) species.

1. Introduction

The impact of long-term exposure to micropollutants on human health is one of today's biggest questions [1]. These pollutants include organic, inorganic, and colloidal species. Pharmaceuticals and personal care products (PPCPs) are new emerging pollutants of high health concerns. PPCPs are widely used to prevent and cure diseases, maintain daily hygiene, and improve lifestyle. Because of their incomplete metabolism in the body, such pollutants are released, unintentionally, into water resources and pose serious hazards [2–4]. The excessive, and probably the abusive, use of PPCPs in recent years has caused spike in their concentration in surface water; particularly, in heavily populated areas around the globe [2,4,5]. The presence of PPCPs in water, even at low concentrations, is placing risks on humans, animals, and aquatic life [1,6,7]. A precise assessment of the health effects of these pollutants is not straightforward [1,7]. This is because of the complicated behavior of PPCPs and their presence with other types of pollutants. Yet, there is increasing evidence for their risks that include, antibiotic resistance, endocrine disruption, allergies, cancer, and reproductive dysfunctions [6,8,9].

Metformin (*N,N*-dimethylbiguanide) is one of the most prescribed drugs to treat Type II diabetes worldwide [5–7,10]. The drug was first synthesized by Werner and Bell in the 1920's and is recently attracting more attention due to its potential anticancer effects [2,11–13]. Metformin is not completely metabolized in the body and leaks into the effluents of wastewater treatment plants (WWTP), as it cannot be removed by the conventional treatment processes. The drug was detected in many WWTP in Canada, USA, Australia, China, and several European countries [6,7,14]. Recently, the FDA recalled batches of metformin for possible N-nitrosodimethylamine (NDMA) contaminations [15]. NDMA is a highly volatile and toxic byproduct of metformin decomposition and was detected in our recent experiments on the oxy-cracking of metformin [16].

Metformin, along with its major transformation product generally urea, have been shown to cause endocrine disrupting in fish, as well as threatening the fertility of male *minnows* [9,14,8]. Recently, it has been shown that metformin can cause severe aggressive behavior in *B. splendens*, at concentrations as low as 40 ppm [17]. There are

* Corresponding author.
E-mail address: nassar@ucalgary.ca (N.N. Nassar).

https://doi.org/10.1016/j.tca.2020.178797
Received 6 July 2020; Received in revised form 5 October 2020; Accepted 5 October 2020
Available online 11 October 2020

increasing voices calling to improve the way we treat wastewater in order to eliminate pollutants including metformin [17,18]. Currently, there are even calls for a "Zero Liquid Discharge" (ZLD) management strategy, which *eliminates* micropollutants in WWTP [19].

Adsorptive removal of pharmaceutical compounds is a common technique to treat wastewater from such pollutants. Recently, metformin was successfully removed from water by using different types of adsorbents including activated carbon [10], graphene oxide [8], and functionalized nanoparticles [20]. Despite the advantages of adsorption as a treatment technique, the process returns a solid waste concentrated on the adsorbent surface, leading to a secondary environmental problem. To overcome these challenges, our group has recently developed a method for removing contaminants from water bodies using environmentally sound micro and nanoparticles [6,21–24]. This could be accomplished by separating the PPCPs from the aqueous media by adsorbing them onto adsorbent-catalyst micro/nanoparticles, which can subsequently promote the decomposition and/or conversion of the adsorbed species. We refer to this unique class of functional micro/-nanomaterials as "nanosorbcats." Capturing the pharmaceutical organic contaminants, like metformin, on nanosorbcats can provide several benefits. Firstly, these materials will increase process performance and efficiency to meet ZLD policy. Secondly, after adsorption, the catalytic conversion will enhance PPCPs properties to form useable materials as they can be converted into small fragments of nitrogen-rich species including ammonia, amines, amidines, and urea derivatives which improve their biodegradability. The catalytic conversion of the PPCPs can be enhanced by thermal process (heat), air (oxidation), steam (partial oxidation) or light (photolysis).

Hence, to advance the *nanosorbcat* concept for treatment of pharmaceutical pollutants, the thermal decomposition of metformin was recently investigated [25]. The study involved a thermogravimetric analysis of the drug under inert conditions and in the absence of any catalyst. With the help of *ab-initio* theoretical calculations, the study showed that metformin thermal decomposition is ruled by methyl radical formations *via* N—CH_3 bond ruptures, and ammonia formation *via* 1,3-H shift mechanism. The decomposition then propagates to form smaller amines, amides, and other nitrogenated species.

In continuation of the previous work [25], herein, the thermo-oxidative decomposition of metformin is investigated under air atmosphere using a thermal analyzer coupled with mass spectrometer (TGA/MS). Such technique was proven to provide important data that can be used to study reaction kinetics and mechanism using isoconversional methods like Kissinger-Akahira-Sunose (KAS) and Friedman (FR) [18,26,27]. Recently, Sbirrazzuoli et al., have developed a method to determine the kinetic parameters for heterogenous reactions using a model-free way [61,62]. Most isoconversional kinetics studies do focus on polymers and ionic solids or liquids, where our attention is geared towards investigating nitrogen-containing compounds, such as metformin, where the thermal oxidation is still poorly understood.

To address the thermo-oxidative reaction mechanism for metformin, high-level density functional theory (DFT) and Møller–Plesset perturbation theory (MP2) calculations were performed as well. The oxidation of metformin was investigated theoretically in the presence of both atomic and molecular oxygen in their *triplet* ground states. Here we provided insights into the reaction mechanism of metformin and the expected products formed under such conditions. This is in line with our continuous efforts to construct a full model to upgrade nitrogen-containing waste into carbon-free fuel (like ammonia) and/or commodity products.

2. Experimental details

2.1. Materials

Metformin (*N,N*-dimethylbiguanide), 99.9 %, was obtained from Sigma-Aldrich, Toronto, Ontario, Canada. Air of UHP grade was purchased from Praxair, Calgary, Alberta, Canada.

2.2. Thermogravimetric/mass spectrometric analysis (TGA/MS)

The thermo-oxidative decomposition of metformin was carried out using thermogravimetric analysis (TGA) [28] with a simultaneous thermal analyzer (Q500, TA Instruments, Inc., New Castle, DE). In a typical experiment, about 15 mg of metformin powder was heated under air from room temperature to 800 °C at different heating rates of 5, 7, 10, and 30 K/min, under continuous air flow of 100 mL/min. A high flow rate of the air was maintained during the experiment in order to minimize any partial pressure effects of the gaseous products on the reaction kinetics [29]. The TGA setup was also attached to an online mass spectrometer (MS) (Pfeiffer Vacuum GSD 301 O_2, Omnistar, Deutschland) using 4-inches long, 1/8 stainless steel tubing to analyze the evolved gases during oxidation of metformin at a heating rate of 5 K/min. This tubing was heated to *ca.* 250 °C using heating tapes to prevent any condensation of the volatiles and gases formed during the experiment. Differential thermal analysis (DTA) was obtained for each thermogram by taking the first derivative of the TGA curve. Further analysis and data treatment were performed using OriginPro 2020 [30]. The TGA instrument was calibrated using zinc as reference material, and each run was repeated three times to confirm the reproducibility of the experiments for the isoconversional computational calculations.

2.3. Theoretical calculations

The details of theoretical calculations were described in previous publications [16,25,31]. In brief, optimized structures for metformin and all possible products or intermediates were obtained using the density functional B3LYP [32] along with the 6−31+G(d,p) basis sets. This level of theory proved to provide good results with metformin and other similar systems [16,25]. The *singlet* ground state was assumed for all closed-shell species. For O_2 and O atom, the *triplet* ground state was used. Here the *triplet* state of molecular oxygen ($^3\Sigma_g$) is donated as O_2(t) for simplicity. Similarly, *triplet* atomic oxygen (^{3}P) is donated as O(t).

Upon a successful optimization, frequency calculations were requested under the same level of theory to authenticate the minimum energy structures. The transition states shown in this work were located either by optimizing good *guesses* of potential structures or by exploring the potential energy scan (PES) for the desired reaction. All transition states were checked to have one and only one imaginary frequency in the direction of the desired reaction coordinate. Zero-point energies (ZPE) were scaled by a factor of 0.9806 as suggested by Scott and Radom [33]. Final single energies were computed using the 2nd order Møller–Plesset perturbation theory (MP2) with the 6−311+G(d,p) basis sets [34,35]. Further details on the calculations of the thermochemical parameters, namely: enthalpy, entropy, and Gibbs free energy involved in this work can be found elsewhere [16,25,31]. All calculations were performed using Gaussian 16 [36] and viewed on Gaussview [37].

3. Results and discussion

3.1. TGA/MS experiments

TGA thermograms and heat flow for neat metformin thermo-oxidative decomposition are shown in Fig. 1. As seen, the decomposition of metformin proceeds with multiple mass losses in the range of 200–650 °C accompanying changes in heat flow (red line) [28]. The first sharp endothermic peak agrees well with the melting point of metformin at 222 °C [38]. The next mass losses and their corresponding peaks are tabulated in Table 1. Under air atmosphere, no exothermic peaks appear up to around 500 °C. This suggests that neat metformin is thermally decomposing in the medium temperature range of 200–500 °C, and the actual oxidation does not start before 500 °C. The first mass loss of 13 % between 225 and 250 °C was observed in our recent study on metformin

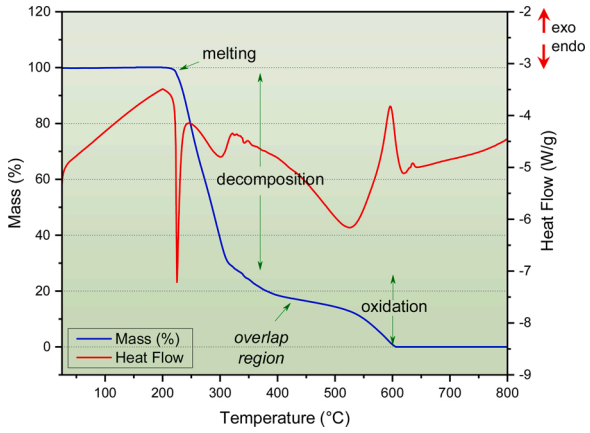

Fig. 1. TGA thermogram for metformin oxidation at airflow of 100 ml/min and heating rate of 5 K/min. Mass (%) = blue, heat flow = red. (For interpretation of the references to colour in this figure legend, the reader is referred to the web version of this article).

Table 1
TGA analysis of metformin oxidation.

Step	Temperature (°C)	Mass loss (%)	Heat flow profile	Process
1	200–225	1.8	Sharp Endotherm	Melting (222 °C) and loss of adsorbed moisture
2	225–250	13.8	Broad Endotherm	Decomposition
3	250–290	33.5	Small endotherm	Decomposition
4	290–350	24.0	Small endotherm	Decomposition
5	350–450	9.1	Small endotherm	Decomposition
6	450–650	17.8	Exotherm	Oxidation

under inert environment [25]. These findings are also evidenced in Fig. 2 which shows the plots of conversion degree (α) against temperature for non-isothermal oxidation at four heating rates (5, 7, 10, and 30 K/min). The extent of conversion (α) ranges between 0 and 1 and is defined as:

$$\alpha = \frac{m_0 - m_t}{m_0 - m_f} \quad (1)$$

where m_0 is the initial sample mass, m_f is the final mass and $m_t$is the mass at a given time.

As seen, the thermo-oxidative decomposition is shifted gradually to the lower temperature by decreasing the heating rate. At a low heating rate (5 K/min), the oxidation starts at 450 °C and is completed by 600 °C, while about 35 % of metformin was oxidized at that temperature (600 °C), at the highest heating rate of (30 K/min). Fig. 2 also shows that the evolution of α with temperature passes through two main regions separated by overlaps near 380 °C and 580 °C. This is accompanied by the appearance of an exothermic peak around 600 °C (Fig. 1). This suggests that the thermo-oxidative decomposition mechanism of metformin involves the following steps, rapid melting, thermal decomposition, an overlap region (*i.e.*, indicating the total reaction effect in this region is the same and is independent of the heating rate), and oxidation.

In addition to the TGA/DTA data, the gaseous products evolved during the TGA experiments were detected by mass spectrometry as explained in the experimental section. Fig. 3 shows the mass profiles for the major mass peaks observed during the study as a function of temperature. Generally, the evolution of the mass peaks is observed between 250 and 600 °C in agreement with the TGA findings. Some of these mass peaks, such as those at m/e 15, 16, and 17 were observed in our recent work on the pyrolysis of metformin [25]. Some of them, however, are new. In the following sections, we discuss the thermo-oxidative mechanisms of metformin based on an isoconversional kinetics model, followed by a quantum theoretical study.

3.2. Kinetics of the thermo-oxidative decomposition of neat metformin

The isoconversional analysis was conducted using the TGA data to estimate the effective activation energy, $E_{\alpha,}$ of metformin thermo-oxidative decomposition reaction. This method demonstrates that the reaction rate at constant conversion (α) is a function of temperature and the state, and hence, it describes the thermo-oxidative reaction kinetics by using multiple single-step kinetic equations, each of which is associated with a certain α and a narrow temperature range at the given α. For the case of linear multiple heating rates, the non-isothermal overall rate of an oxidation reaction for a condensed phase can be described by Eq. (2) [39,29]:

$$\frac{d\alpha}{dT} = (A_\alpha/\beta)\exp\left(\frac{-E_\alpha}{RT}\right)f(\alpha) \quad (2)$$

where T is the reaction temperature, E_α is the effective activation energy for a constant conversion, A_α is the pre-exponential factor, $\beta = \frac{dT}{dt}$ is the heating rate, R is the ideal gas constant, α is the extent of conversion, and $f(\alpha)$ is the reaction model which depends on a particular mechanism. α can be calculated from thermogravimetric analysis using Eq. (1).

Several differentials and integral isoconversional methods were reported to estimate E_α [40]. Here, we estimated the values of E_α using multiple heating rates (5, 7, 10 and 30 K/min) following the differential

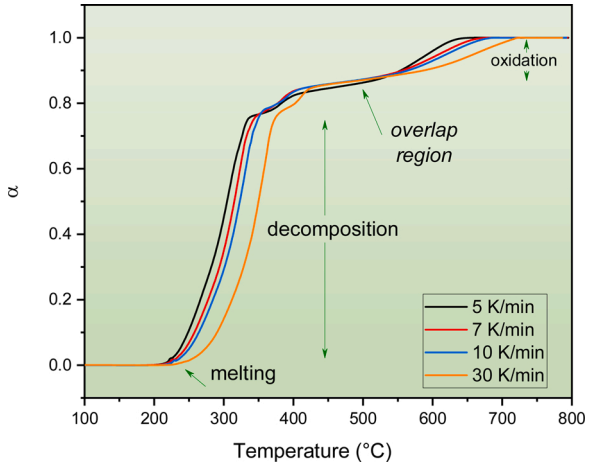

Fig. 2. The extent of conversion (α) as a function of temperature at different heating rates under an airflow of 100 mL/min.

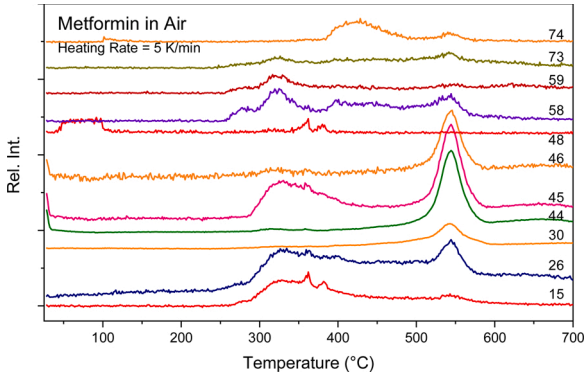

Fig. 3. Mass spectrometric profiles of major products obtained during metformin oxidation under air atmosphere.

methods of Friedman (FR) [41] and the integral method of Kissinger-Akahira-Sunose (KAS) [42,43]. The advantage of using FR is that it uses no approximation like KAS, and can be applied to any temperature program which can be obtained by taking the logarithms of both sides of Eq. (2) under different heating protocols (β_i) as follows

$$ln\left(\beta_i\frac{d\alpha}{dT}\right) = -\frac{E_\alpha}{RT_i} + ln(A_\alpha) + lnf(\alpha) \quad (3)$$

where β_i is the heating rate, $\beta_i = dT/dt$, for linear non-isothermal reaction [44]. The index (i) denotes various temperature programs, T_i is the temperature at which the given conversion degree (α) is achieved under the corresponding heating rate. By applying this principle, the term $\ln(A_\alpha) + \ln f(\alpha)$ remains unchanged for a given (α). Thus, E_α is estimated from the slope of the best-fit line of the plot $\ln(\beta_i\frac{d\alpha}{dT})$ against $(\frac{1}{T_i})$. Furthermore, the reaction model, $f(\alpha)$, can be obtained through linear regression of $\ln(\beta_i\frac{d\alpha}{dT})$ against $\ln f(\alpha)$ for some previously proposed models, as detailed elsewhere [29,39,45,46].

For the case of KAS integral method, upon the integration of Eq. (2). and rearranging, we can obtain:

$$g(\alpha) = \int_0^\alpha \frac{d\alpha}{f(\alpha)} = \left(\frac{A_\alpha}{\beta}\right)\int_0^T \exp\left(\frac{-E_\alpha}{RT}\right)dT \quad (4)$$

Eq. (4). represents a nonsolvable integration by the analytical method in closed form [29]. Using the series approximation ($p(x) \cong e^{-x}/x^2$), the KAS equation becomes [42,43]:

$$ln\left(\frac{\beta_i}{T_{\alpha,i}^2}\right) = \ln\left(-\frac{A_\alpha R}{E_\alpha}\right) - \ln g(\alpha) - \left(\frac{E_\alpha}{RT_{\alpha,i}}\right) \quad (5)$$

where $g(\alpha)$ is the integral form of the reaction model ($f(\alpha)$). Hence, the effective activation energies can be estimated from the plot of the left side of Eq. (5) against $1/T_{\alpha,i}$ at constant α for β_i.

Fig. 4-a shows the linear Arrhenius fittings for the thermo-oxidative decomposition of metformin in air according to the FR method (eq. 3). Similar plots were obtained for the KAS method and are presented in Fig. S1. The R^2 regression values were very close to unity within the α range of 0.05 – 0.95, except for the region 0.80−0.90, where an overlap was observed (*cf.* Fig. 2). The isoconversional method cannot be applied in this region as the method is used only for estimating the data sets within well-separated steps. The effective activation energies were obtained from the slopes of the linear fittings according to Eqs. (3) or (5). The dependence of the E_α on α for both the FR and KAS Eqs is shown in Fig. 4-b. The deviations in E_α values obtained from KAS and FR can be explained by the fact that the differential isoconversional methods, like FR, are proven to be sensitive to experimental noise, resulting in deviations of E_α, which limits its application in assessing condensed phase reactions [40]. In the KAS method, which is derived based on the constant E_α, the error associated with kinetic values is dependent on the variation of the effective activation energy with conversion which is not the case in FR method. Additionally, the obtained values of effective activation energies by FR are independent on the heating rate, which gives another advantage for FR by reducing the systematic error in evaluating the activation energy values. The good performance of the FR method was evident in DSC simulations by Sbirrazzuoli et al. [60].

Clearly, the effective activation energy is increasing with the extent of conversion for both KAS and FR. The variation of E_α with α can be explained in terms of the individual steps for the overall decompaction of the reactants [29,39]. For a simple single-step gas-phase reaction, the activation energy is conventionally described by a single barrier that can be determined from the energy difference between the reactants and the activated complex. But for a condensed phase process, such as in our case, the reaction involves a heterogeneous interaction between the solid matter and gaseous species (O_2, O, OH) and is way more complicated to be expressed in a single step. Therefore, the use of isoconversional methods to express the reaction kinetics becomes valuable.

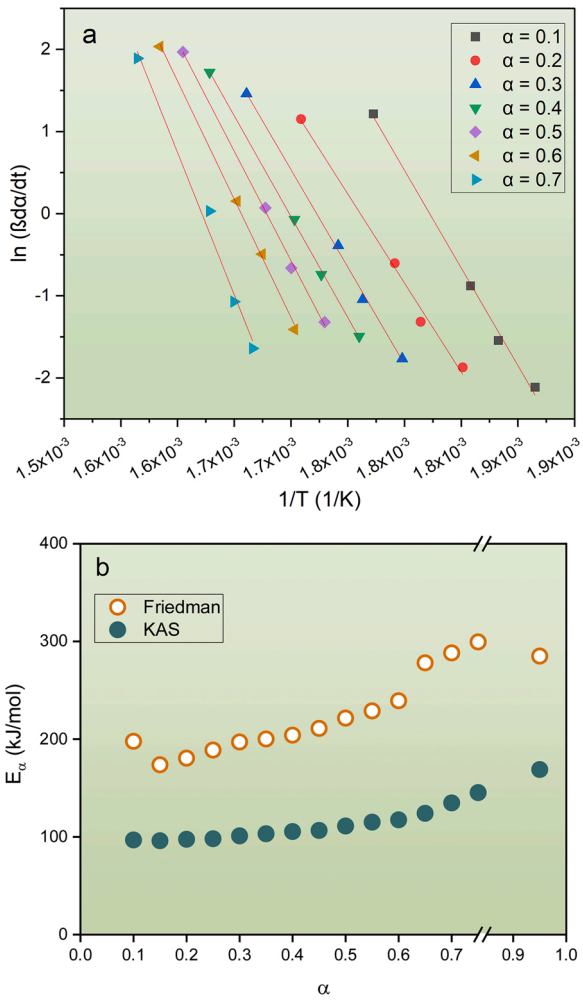

Fig. 4. a) Arrhenius fittings for the thermo-oxidative decomposition of metformin in air according to the FR method (For KAS, see Fig. S1) b) dependence of the effective activation energy on extent of reaction conversion α using KAS and FR methods.

The experimental E_α values for metformin decomposition start with *ca.* 100 (KAS) and 200 (FR) kJ/mol and increase with α. Recall that at temperatures below 500 °C (α ≈ 0.8), no exothermic peaks were observed as shown in Fig. 1. Rather, few endothermic peaks were observed, as shown in Table 1 (Steps 1–4). This infers that no oxidation takes place at this stage and metformin undergoes neat thermal decomposition. Typical activation energy values for the thermal decomposition of organic compounds, including bond dissociation energies of those in metformin, are > 200 kJ/mol [47]. Therefore, the FR results sound more practical, in support of the advantage of FR over KAS mentioned earlier, and the results obtained by Sbirrazzuoli et. al [60]. This is also supported by the results obtained from our recent work [25]; when N_2 was used as a purging gas, the mass loss of 13.8 % (*cf.* Table 2) was attributed to the formation of ammonia or methyl radical, which both contribute to about 13 % of metformin total molecular mass [25]. The formation of ammonia was explained by a 1,3-H shift from the -NH group to the NH_2 terminal in metformin. The theoretical activation energy (in terms of $\Delta G^{\circ\ddagger}$) for this shift was estimated at 257.4 kJ/mol [25]. In addition, the thermal decomposition of metformin involved some other homolytic bond ruptures to form reactive radicals, that initiated secondary free-radical chain reactions. The theoretical values of E_α's for these reactions were ranging between 250 and 410 kJ/mol. These theoretical E_α values are closer to those obtained from the FR model than KAS. Nonetheless, the experimental E_α's determined in

Table 2
Kinetic parameters obtained by combining Friedman equation with model fitting.

α	T (°C)	$f(\alpha)$	Slope	R^2	A_α (s^{-1})	$\Delta S^{\ddagger}$ (J/K.mol)	$\Delta H^{\ddagger}$ (kJ/mol)	$\Delta G^{\ddagger}$ (kJ/mol)
0.25	274	$3/2(1-\alpha)^{2/3}[1-(1-\alpha)^{1/3}]^{-1}$	1.38	0.9876	1.06×10^{16}	48.5	186.5	160.0
0.5	305	$3/2(1-\alpha)^{2/3}[1-(1-\alpha)^{1/3}]^{-1}$	1.42	0.9904	5.78×10^{18}	100.4	219.0	160.9

Fig. 4-b are lower than the theoretical values determined in our recent study [25]. This can be explained by the fact that the theoretical $\Delta G^{\circ\ddagger}$ values were computed at room temperature and 1 bar in the gas phase. The experimental conditions of our study were at much higher temperatures, and involve heterogeneous interactions as mentioned earlier, that can alter the reaction mechanism [48,49].

Based on the above discussion, we conclude that the E_α's for $0.1 < \alpha < 0.75$ does correspond to the decomposition region (*cf.* Fig. 2), and those between $0.85 < \alpha < 0.95$ can be attributed to oxidation. The oxidation E_α is obviously higher than the decomposition due to the fact that oxidation requires higher activation barrier, as explained later in the theoretical calculations part. According to Fig. 4-b, the experimental E_α's obtained in this work have ranged from 100 to 145 kJ/mol and 200–300 kJ/mol for the KAS and FR methods, respectively.

3.3. Determination of the most probable mechanism function, pre-exponential factor and reaction order

The isoconversional method can also be used to determine the reaction model, $f(\alpha)$. as per Eq. (3) [45,29,39]. Consequently, the kinetic triplet, A, and $\Delta S^{\ddagger}$, $\Delta G^{\ddagger}$ can be determined. We used the results of the FR model for this part of the study as it gave more practical results as mentioned earlier. First, the y-intercepts of the linear fittings shown in Fig. 4-a are equaled to $\ln(A_\alpha) + lnf(\alpha)$ according to Eq. (3). So, if one could determine $f(\alpha)$, the pre-exponential factor (A_α) can be determined. Second, At constant temperature, and therefore constant α, Eq. (3) can be also used to find $f(\alpha)$ through a linear fitting between the left side ($\ln(\beta_i \frac{d\alpha}{dT})$ *vs.* $\ln f(\alpha)$ for some known model of $f(\alpha)$. The slope of such fitting would equal to -1 according to Eq. (3). Thus, the data obtained in this experiment were fitted to thirteen different proposed reaction models as proposed by Vyazovkin *et. al.,* [29,39] (Table S1 in Supporting Information), and the best fitting was obtained for a three-dimensional diffusion function, that is represented by:

$$f(\alpha) = 3/2(1-\alpha)^{2/3}\,[1-(1-\alpha)^{1/3}]^{-1} \quad (6)$$

The linear fittings to locate the reaction model were done at $\alpha = 0.25$ and 0.5, and the results are tabulated in Table 2. The closest slopes to unity were found for the above function (Eq. (6)) with R^2 values close to unity as shown in the table. Unfortunately, the attempts to find the reaction model at higher values of α, where the oxidation mechanism takes place, have failed. This is because of the very narrow conversion as shown in Fig. 2. Therefore, the reaction model and the kinetic parameters listed in Table 2 are representing the decomposition region.

3.4. Estimation of kinetic transition state parameters

The temperature-dependent pre-exponential factor (A_α) for the unimolecular decomposition of metformin can be obtained from the y-intercept of Eq. (3) as explained in the previous section, and the reaction model, $f(\alpha)$. According to the transition state theory, A is defined as [50,45].

$$A_{uni} = \left(\frac{ek_BT}{h}\right)e^{\Delta S^{\neq}/R} \quad (7)$$

where e is the Napier's constant (2.7183), k_B is Boltzmann constant, h is Planck's constant, and R is the universal gas constant. Thus, the entropy of activation, $\Delta S^{\neq}$, can be also obtained by rearranging Eq. (7). as follows:

$$\Delta S^{\neq} = R\left(ln\frac{Ah}{ek_BT}\right) \quad (8)$$

The pre-exponential factor (A_α) values deduced from this analysis are shown in Fig. 5. In a similar trend to the effective activation energy, the A_α values also increase with α, stressing that metformin decomposition is a multi-reaction step. The physical meaning of A_α is its reflection on the nature of the transition state, as described by Eq. (7). Large values of A_a correspond to a more relaxed (open) TS [51,31]. The enthalpy of activation ($\Delta H^{\neq}$) was obtained by applying the relationship and $E_\alpha = \Delta H^{\neq} + RT$. Similarly, the Gibbs free energy of activation was obtained from the equation $\Delta G^{\neq} = \Delta H^{\neq} - T\Delta S^{\neq}$.

The results of the reaction model fittings, and the corresponding kinetic parameters, $S^{\neq}$, $\Delta H^{\neq}$, and $\Delta G^{\neq}$, are tabulated in Table 2. The positive values of $\Delta S^{\neq}$ obtained from this analysis indicates a transition state that is more disordered than the state of initial reactants. This usually takes place in unimolecular thermal decompositions where one reactant decomposes into several radicals with a *relaxed* TS [51,25,31]. The outcomes of Table 2 and further explanations of the variation of the activation energy with α will be discussed in the following section using first principle calculations.

3.5. Theoretical calculations

To further explain the oxidation mechanism for neat metformin, an *ab-initio* study was performed as detailed in the theoretical calculations section. It is believed that oxidation of organic molecules can be initiated either by O_2 molecule as well as individual O atoms [46,52–55]. Thus, our theoretical study has involved both. Although both the *singlet* and *triplet* states of oxygen can contribute to the oxidation mechanism, we focus our attention on the *triplet* ground state. This is because excitation, by photochemical or ionization sources, to the *singlet* state is not plausible under the experimental conditions of this work.

First, we consider the H-abstraction from metformin by molecular

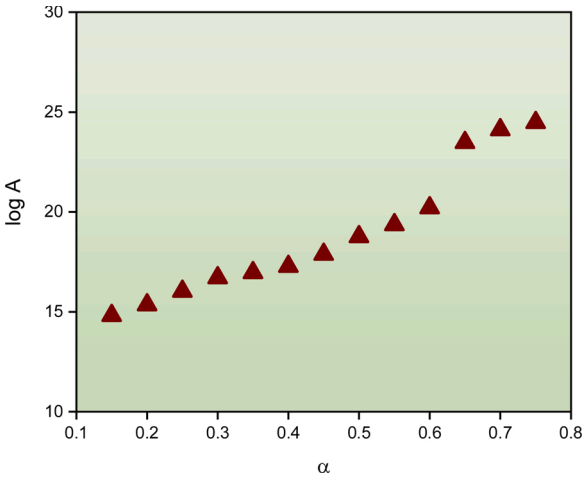

Fig. 5. Pre-exponential factor (A_α) values obtained from the Friedman model, as a function of α.

oxygen as illustrated in Scheme 1. The initial attacks of O_2(t) are taking place on three sites of metformin: —NH, —NH_2, and the —CH_3 groups. As a result, radicals 1–3 as well as $^{\bullet}HO_2$ are formed. The transition states for the three pathways were successfully located at B3LYP/6−31+G(d, p) level of theory and are labelled TS1, TS2, and TS3. The optimized structures for transition states are shown in Fig. S2. The O—O≡H bond distance is *ca.* 1.07 Å in TS1 and TS2, and the N—H bond is elongated from the normal 1.02–1.5 Å. In the case of TS3, the abstraction takes place at 1.09 Å distance and the C—H bond is elongated further from 1.09 to 1.60 Å.

The potential energy diagram for the reactions of mechanism **A** is shown in Fig. 6. The values in the figure represent the Gibbs free energies at room temperature, obtained at Møller–Plesset (MP2) level as detailed in the theoretical section. The activation barriers, in terms of $\Delta G^{\circ\ddagger}$, are equal to 261.9, 302.1, and 224.3 kJ/mol for TS1, TS2, and TS3, respectively. The three reactions are also highly endergonic (non-spontaneous) with ΔG° values of about 220−300 kJ/mol. These values are in agreement with the previously reported values for H abstractions from similar molecules [55,56]. For example, the activation barrier for H abstraction from ammonia by O_2(t) was determined to be 62.5 kcal/mol (261.5 kJ/mol) at CCSD(T)//RMP2 level [56]. The relatively high activation barriers for mechanism **A** can explain the resistance of metformin for oxidation at temperatures lower than 500 °C in our TGA/MS experiments.

Next, we consider the attack of O_2(t) on the carbon atom, C1, as illustrated in Scheme 2. In this mechanism, donated **B**, the attack leads to the formation of the oxygenated radical 4. The transition state (TS4) leading to this radical was located and shown in Fig. S3. From radical 4, the oxidation can take different routes, either by losing -NH_2 to form radical 5 or by breaking the C1-N bond to form radicals 6 and 7. Alternatively, the loss of NH species can form radical 8 as shown in the scheme. All transition states for this mechanism were successfully located and are shown in Fig. S3. The potential energy diagram for this mechanism (Fig. 7) demonstrates a high activation barrier to initiate this mechanism (298.3 kJ/mol). The barriers for proceeding steps to form the final radicals are even higher at 388.7, 397.5, and 443.5 kJ/mol for TS5, TS6, and TS7, respectively. In addition, all these reactions are highly endergonic with ΔG° values in the range of 290−565 kJ/mol. The pathway leading to radical 6 and NH (imidogen) is the least favorable with ΔG° =566.5 kJ/mol. Cleary, this mechanism is associated with higher activation barriers unlike those obtained experimentally in Fig. 4-b. As explained earlier, the theoretical values were obtained at room temperature and in the gas phase, where the actual experimental conditions were under elevated temperatures and heterogenous nature for condensed phase.

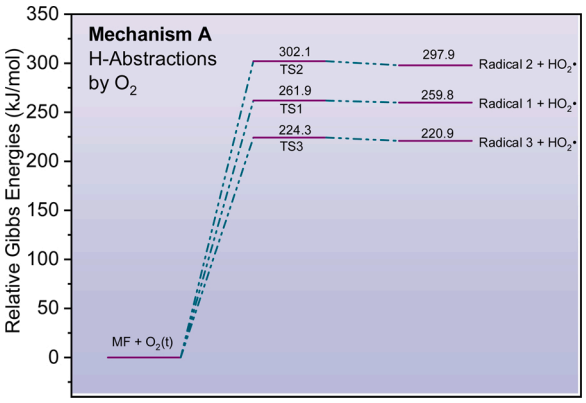

Fig. 6. Potential energy level diagram for the hydrogen abstractions by molecular oxygen, O_2(t). Energies represent relative Gibbs free energies in kJ/mol at 298 K and 1 atm. (ZPE corrections are included).

Mechanism **B** suggests the formation of NH (imidogen) which has a mass of 15 amu. A mass peak at *m/e* 15 was observed between 300 and 400 °C, as shown in Fig. 3. This peak can represent either NH or CH_3 species. In our recent work on metformin pyrolysis [25], the loss of methyl radical from metformin was studied under the same level of theory of this work. The reaction is shown in Scheme 3 and it also leads to the formation of methylbiguanide (MBG) *via* a radical stabilization. The loss of methyl radical through N—CH_3 bond rupture was associated with a 313.8 kJ/mol barrier [25]. This is much less than the barrier for NH formation reported above. Therefore, the mass peak of *m/e* = 15 in our experiment is mostly attributed to CH_3 formation, rather than NH. This is also supported by the fact that the oxidation pathway leading to the formation of NH is unlikely to start at this temperature. It is worth mentioning that Tisler and Zwiener have recently reported that MBG is the major transformation product of metformin in waste and surface waters [14].

In a parallel mechanism to that of **A**, an attack of O_2(t) on C3 in metformin can lead to the formation of radical 9, as illustrated in

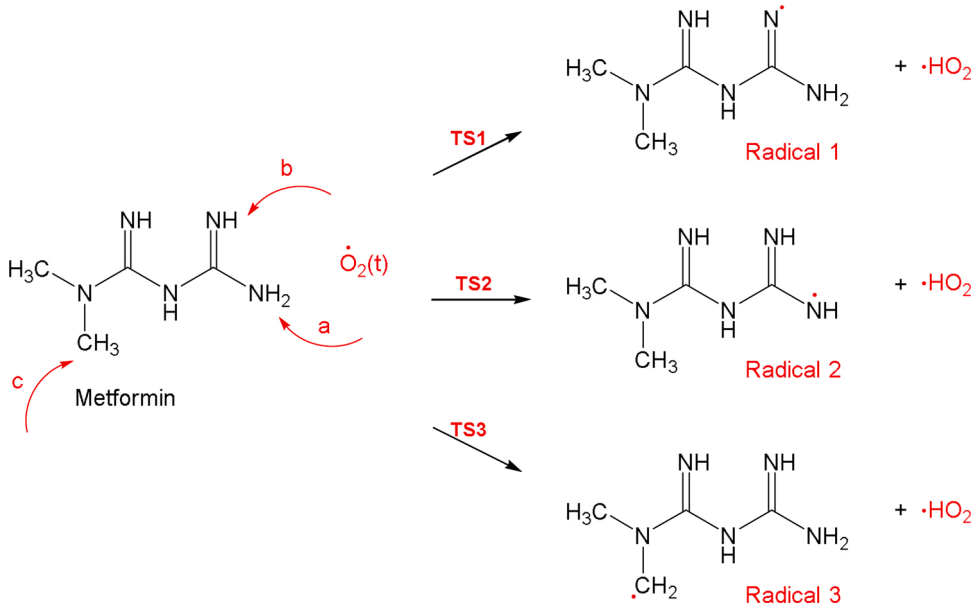

Scheme 1. Reaction mechanism **A**, hydrogen abstractions in metformin by molecular oxygen, O_2(t).

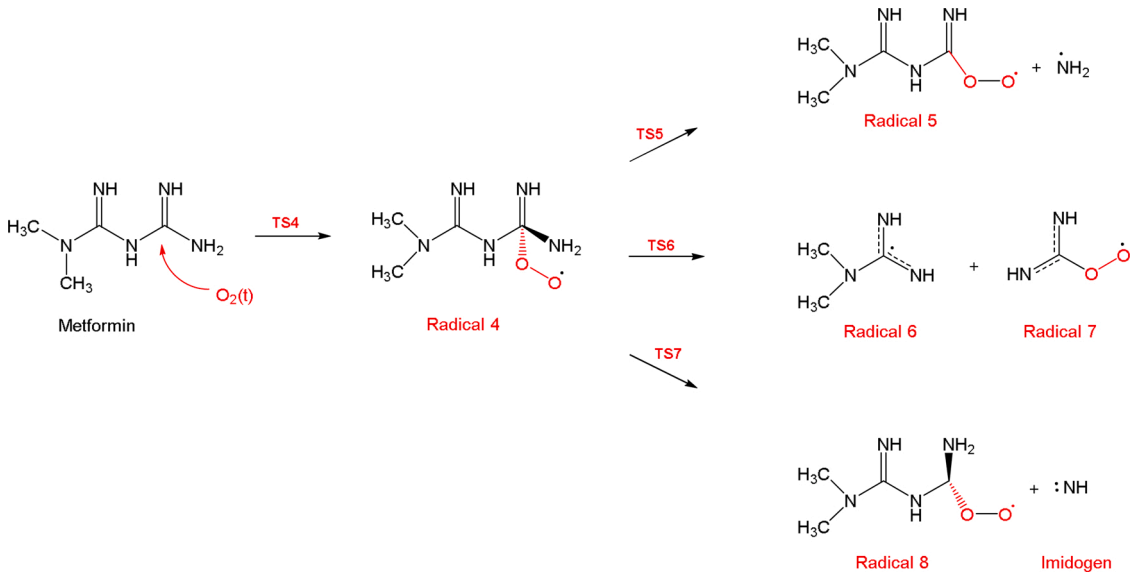

Scheme 2. Metformin reaction mechanism B initiated by O_2(t) attacks on C1.

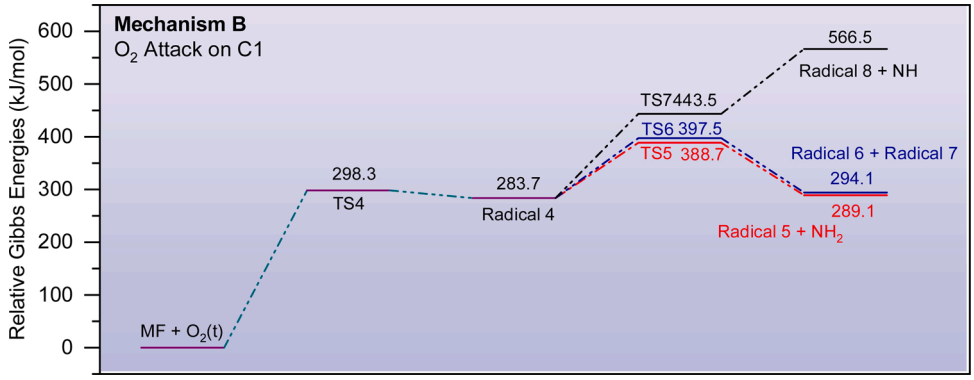

Fig. 7. Potential energy level diagram for reaction mechanism **B** initiated by O_2(t) attacks on C1 in metformin. Energies represent relative Gibbs free energies in kJ/mol at 298 K and 1 atm. (ZPE corrections are included).

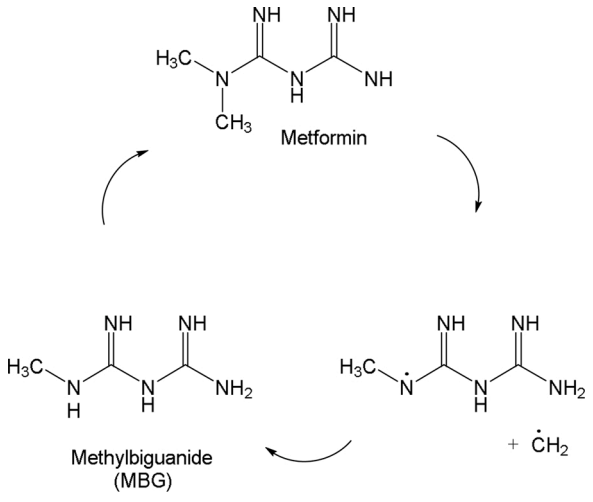

Scheme 3. Formation of methylbiguanide (MBG) from metformin by loss of CH_3 radical.

Scheme 4. The exit pathways for this radical are the formation of dimethylaminyl radical 11 plus radical 10, the radical pairs 12 and 13, and imidogen plus radical 14. During our TGA/MS experiments on metformin, mass peaks at *m/e* 45 and 45 were observed in the temperature range 500–600 °C, as shown in Fig. 3. Those peaks can represent dimethyl amine (DMA, $M = 45$ amu) and it's radical 11. The mass peak at *m/e* 45 was also observed at a cooler temperature (300−400 °C). This indicates that DMA can be formed by neat thermal decomposition as we proposed elsewhere [25], or through the oxidation mechanism **C**. Another experimental evidence for mechanism **C** is the evolution of the mass peaks at *m/e* 58, and 59 as seen in Fig. 3. These peaks can be associated with guanidine and its radical 13.

The optimized structures for all transition states of this mechanism are shown in Fig. S4. As for every transition state in this work, their authenticity was verified by examining their vibrational frequencies and making sure they have a single imaginary frequency in the desired reaction coordinate. The ΔG° values of this mechanism (Fig. 8) are not very different from those of mechanism **B**, indicating that both attacks on C1 and C3 by molecular oxygen are mutually equivalent.

As discussed, the oxidation of metformin by O_2(t) is unfavorable in terms of both values of $\Delta G^{\circ\ddagger}$ and ΔG°. Thus, we considered the reaction of the drug with atomic oxygen in its *triplet* ground state. The following mechanisms are proposed under the assumption that atomic oxygen is forming under the experimental conditions of this work.

Similar to mechanism **A**, atomic oxygen O(t) can initiate the oxidation of metformin by abstracting hydrogens from NH_2 or NH groups to form radicals 1 or 2, in addition to the reactive hydroxyl ($^{\bullet}$OH) radical, as

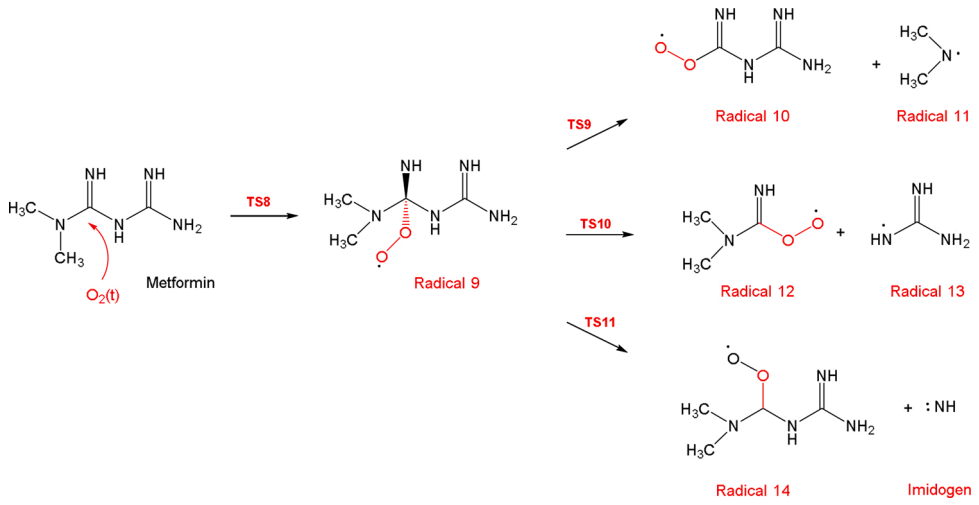

Scheme 4. Metformin reaction mechanism **C** initiated by O_2(t) attacks on C3.

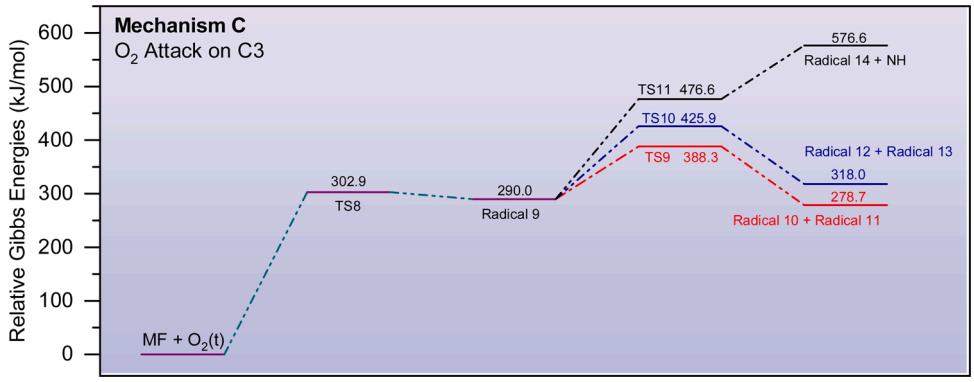

Fig. 8. Potential energy level diagram for reaction mechanism **C** initiated by O_2(t) attacks on C3 in Metformin. Energies represent relative Gibbs free energies in kJ/mol at 298 K and 1 atm. (ZPE corrections are included).

shown in Scheme 5. The hydroxyl radical can itself contribute to the oxidation mechanism. The role of the ˙OH in the oxidation of organic molecules, including metformin, was studied by our group previously [16,46,57]. The two transition states, TS12 and TS13, were located and their optimized structures are shown in Fig. S5. We have not located a transition state for the abstraction of H from the methyl group in metformin using the B3LYP functional. Neither we located such TS using other DFT functionals or MP2 methods.

Out of comparison, the O≡H bond distance in TS13 is 1.26 Å, and the N—H bond is elongated to 1.19 Å, whereby the values in TS2 were 1.07 and 1.5 Å, respectively. Thus, the O(t) atom is closer to the H being abstracted than in the case of O_2(t). This reflects the reactivity of O(t) towards H-abstraction, and consequently, the lower activation barrier of abstraction. As seen in Fig. 9, both $\Delta G^{\circ\ddagger}$ and ΔG° are much less than those of molecular oxygen. Also, the H abstraction from the -NH site is

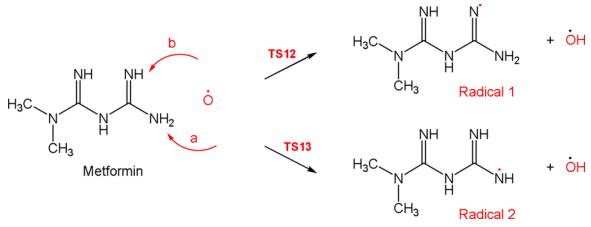

Scheme 5. Reaction mechanism **D**, hydrogen abstractions in Metformin by atomic oxygen, O(t).

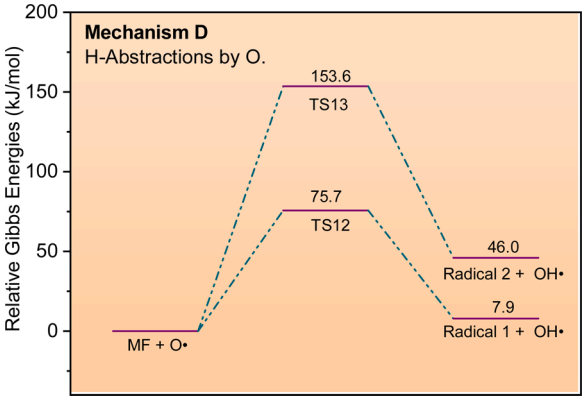

Fig. 9. Potential energy level diagram for the hydrogen abstractions by atomic oxygen, O(t). Energies represent relative Gibbs free energies in kJ/mol at 298 K and 1 atm. (ZPE corrections are included).

much more favorable than that from —NH_2; $\Delta G^{\circ\ddagger}$ and ΔG° are as low as 75.7 and 7.9 kJ/mol, respectively (Figs. 10 and 11).

The attack of O(t) atom on C1 and C3 in metformin is illustrated in Schemes 6 and 7, respectively. The reaction mechanism takes similar pathways to that of O_2(t). The radicals 15 and 19 are formed first, followed by their decomposition into different sets of products. Some of these radical products can stabilize to form some familiar transformation products of metformin. For example, dimethyl amine (11),

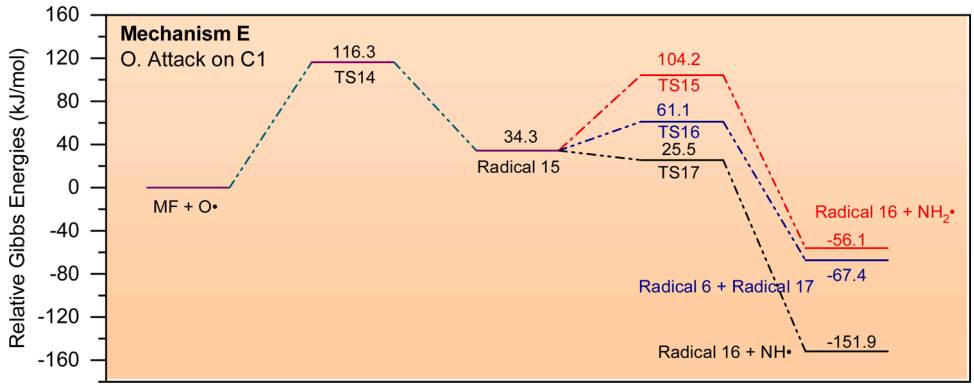

Fig. 10. Potential energy level diagram for reaction mechanism E initiated by O(t) attacks on C1 in Metformin. Energies represent relative Gibbs free energies in kJ/mol at 298 K and 1 atm. (ZPE corrections are included).

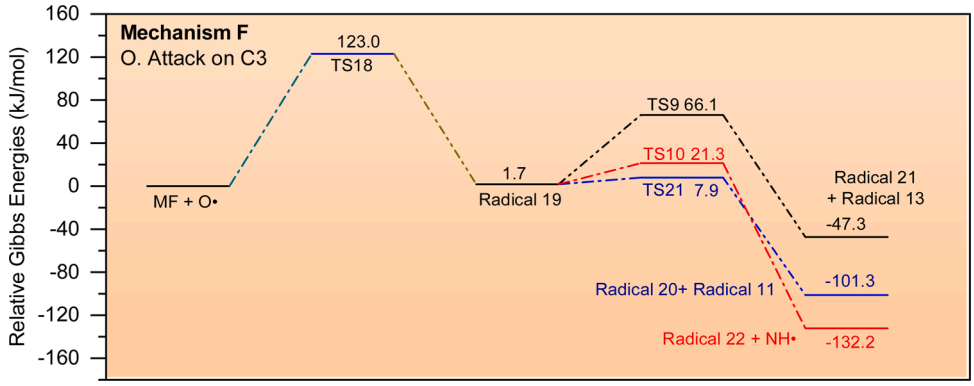

Fig. 11. Potential energy level diagram for reaction mechanism F initiated by O(t) attacks on C3 in metformin. Energies represent relative Gibbs free energies in kJ/mol at 298 K and 1 atm. (ZPE corrections are included).

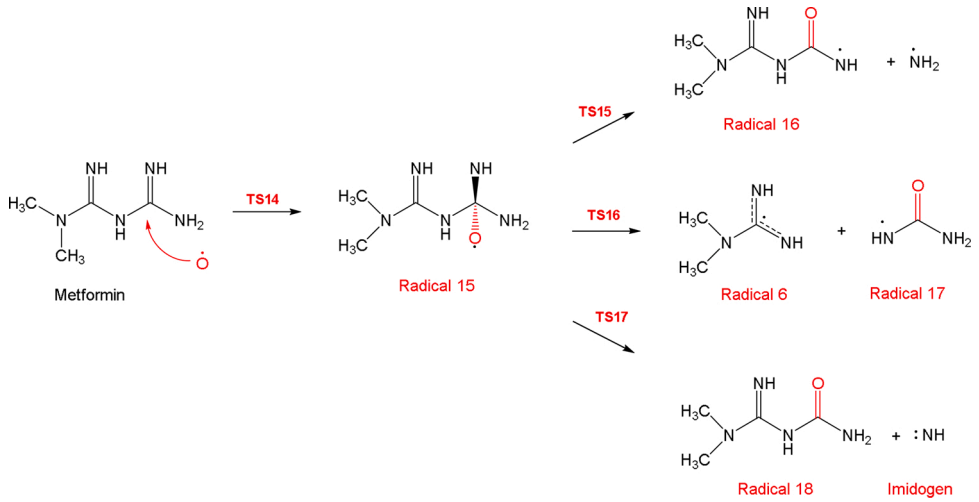

Scheme 6. Metformin reaction mechanism **E** initiated by O(t) attacks on C1.

urea (radical 17), and dimethyl urea (radical 21) were all detected during our recent work on the oxy-cracking of metformin [16]. Also, the mass peak at m/e 59 in this work (*see* Fig. 3) can be attributed to the urea radical 17.

The transition states for these two mechanisms, **E**, and **F**, are all shown in Figs. S6 and S7, respectively. The energy diagrams are also shown in Fig. 12. Generally, the $\Delta G^{\circ\ddagger}$ and ΔG° values of metformin reactions with O(t) are lower than those that those of O_2(t).

Finally, we considered the O(t) atom attack on the NH and NH_2 groups in metformin. All attempts to locate a transition state for the NH_2 pathway were failed. All the PES scans we performed in order to locate such TS's ended with a cusp in the reaction coordinate, indicating that such TS does not exist under the level of theory of this work. Nevertheless, we located the TS for the NH pathway and the reaction mechanism is illustrated in Scheme 8. Upon the formation of radical 23, the exit products are either radical 24 and azanone, or the radical pairs 6 and 25. the transition states for this mechanism are shown in Fig. S8. The potential energy diagram is also shown in Fig. 12. This type of attack is

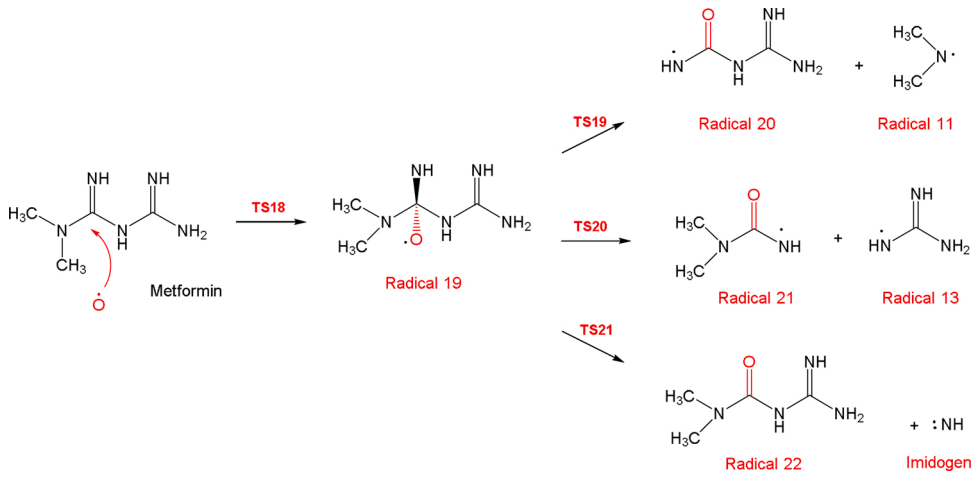

Scheme 7. Metformin reaction mechanism **F** initiated by O(t) attacks on C3.

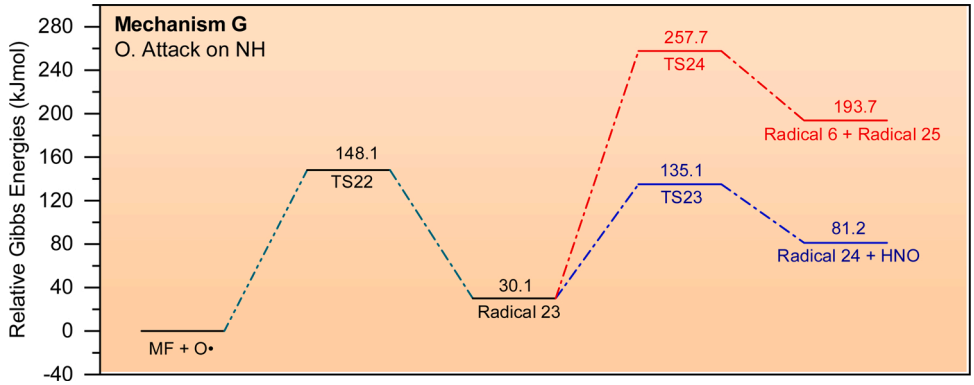

Fig. 12. Potential energy level diagram for reaction mechanism **G** initiated by O(t) attacks on NH in metformin. Energies represent relative Gibbs free energies in kJ/mol at 298 K and 1 atm. (ZPE corrections are included).

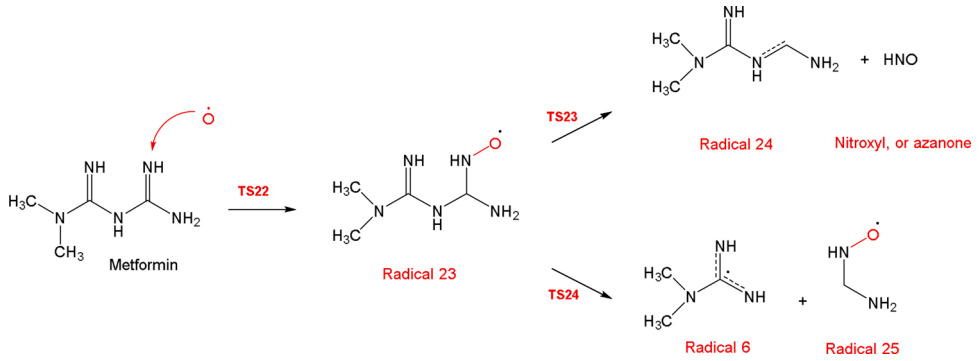

Scheme 8. Reaction mechanism **G** initiated by O(t) attacks on NH in Metformin.

associated with much higher $\Delta G^{\circ\ddagger}$ and ΔG°, values, which makes it an unfavorable pathway. This is supported by the fact that no mass peaks were observed in our TGA experiments that correspond to the products of this mechanism.

3.6. The competition between O_2(t) and O(t)

In the previous section, the oxidation reactions of metformin in the presence of O_2(t) or O(t) were presented. It was concluded that the reactions with O(t) atom were associated with lower $\Delta G^{\circ\ddagger}$ and ΔG° values compared to those of O_2(t) molecule. To better understand this competition, we summarize the primary reactions of metformin with

Table 3
Summary of the metformin primary reactions with O_2(t) and O(t).

Mechanism	Reactants	Products	$\Delta G^{\ddagger}$ (kJ/mol)	ΔG° (kJ/mol)
A	MF + O_2(t)	Radical 1 + $^{\bullet}HO_2$	261.9	259.8
A	MF + O_2(t)	Radical 2 + $^{\bullet}HO_2$	302.1	297.9
A	MF + O_2(t)	Radical 3 + $^{\bullet}HO_2$	224.3	220.9
B	MF + O_2(t)	Radical 4	298.3	283.7
C	MF + O_2(t)	Radical 9	302.9	290.0
D	MF + O(t)	Radical 1 + $^{\bullet}OH$	75.7	7.9
D	MF + O(t)	Radical 2 + $^{\bullet}OH$	153.6	46.0
E	MF + O(t)	Radical 15	118.3	34.3
F	MF + O(t)	Radical 19	123.0	1.7

both species in Table 3. Here, we only consider the first primary attacks that are responsible for initiating the oxidation reactions. When the H-abstraction mechanism **A**, for O_2(t), is compared with that of O(t), mechanism **D**, the latter seems to be more favorable in terms of both $\Delta G^{\circ\ddagger}$ and ΔG°. A similar trend can be observed when the O_2(t) mechanisms **B**, and **C** are compared to those of O(t), (**E**, and **F**). This might deceive us to conclude that O(t) reactions are more favorable. There is no doubt that O(t) is much more reactive than O_2(t). However, the reactions with O(t) requires the rapture of the O═O bond, which can only take place at high temperatures. The reported O═O bond dissociation energy is 498 kJ/mol [58]. If this value is taken into account, the activation barriers of the O(t) pathways become very high, and therefore less favorable than those of O_2(t).

Recall that the experimental value of E_α determined from the isoconversional method of Friedman was in the range of 200−300 kJ/mol. This value is within the range of the calculated $\Delta G^{\ddagger}$ values for the O_2(t) attacks. This supports the notion that metformin oxidation is dominated by O_2(t) attacks rather than atomic oxygen.

3.7. Explaining the variation in the effective activation energy

We demonstrated that the thermo-oxidative decomposition of metformin proceeds in four major mechanisms, melting, decomposition, an overlap region, and oxidation. According to our results (*cf.* Figs. 2 and 4), the experimental E_α values for $0.1 < \alpha < 0.75$ correspond to the decomposition region, while those for $0.85 < \alpha < 0.95$ are attributed to oxidation. The experimental $\Delta G^{\ddagger}$ value (for both $\alpha = 0.25$ and 0.5) that is attributed to decomposition was estimated at 160 kJ/mol (*cf.* Table 2). This value lies within the theoretical values for the thermal decomposition of metformin obtained in our recent work [25]. On the other hand, no $\Delta G^{\ddagger}$ value could be determined for the oxidation region. But the estimated E_α of oxidation ranges between 280 and 420 kJ/mol, which lies within the calculated values of O_2(t) attacks, according to our calculations.

The results of this work demonstrate a variation of the experimental E_α with α. Two questions can arise here; what is the cause of this variation? and why the experimental E_α values are different than the calculated ones. According to Vyazovkin et.al, variable effective activation energy is physically meaningful "*as long as it can be explained in terms of the activation energies for individual steps of the overall process*" [29,39]. Therefore, the answer to the first of these two questions is that metformin first decomposes thermally between 200−500 °C (α = 0.0–0.8) through several possible decomposition pathways, as detailed in our recent work [25]. Next, metformin undergoes thermal oxidation between 500−700 °C (α = 0.8–1.0) with the readily available oxygen molecules. The primary oxidations produce the intermediate radicals shown across the manuscript, *e.g.* radicals 1–4, and 9. These radicals can further oxidize and initiate further reactions with their activation barriers.

As for the second question, we indicated that the oxidation of metformin in our experiments is a heterogenous process where the reaction zone is the interface between the solid matter and the gaseous oxygen [29]. Under such conditions, the reaction is far away from the conventional model of a homogeneous single-step reaction, where two reactants are mixed at the molecular level. This realization, along with the fact that the theoretical values obtained in this work were computed at room temperature and 1 bar in the gas phase, In addition, the activation barriers are expressed in terms of $\Delta G^{\ddagger}$, which include an enthalpy as well as an entropy term ($\Delta G^{\ddagger}=\Delta H^{\ddagger}$-T$\Delta S^{\ddagger}$) and are expected to be slightly temperature dependent. We demonstrated such dependence in previous works for several organic molecules [46,51]. Typically, the activation enthalpy ($\Delta H^{\ddagger}$) does not change significantly with temperature. However, $\Delta S^{\ddagger}$ can be severely affected by temperature variations particularly when the translational entropy change is large. For instance, reactions that involve two reactants and one TS (A + B→TS→P) have a higher change in translational entropy than single decompaction reactions (A→TS→P) [51,59]. This variation of $\Delta S^{\ddagger}$ with temperature can contribute to the $\Delta G^{\ddagger}$ variation, which explains the change of E_α with α.

4. Conclusions

The kinetics of the thermo-oxidative decomposition of metformin was studied by thermogravimetry coupled to MS analysis and theoretical calculations. The study revealed that the thermo-oxidative decomposition of the drug proceeds by a rapid melting, followed by thermal decomposition, and finally by complete oxidation at 700 °C. An overlap region was detected between the last two steps. The decomposition started at 200 °C with the loss of ammonia and methyl radical formation. At *ca.* 500 °C, oxidation of the drug starts and produces several gaseous products.; some of which are known transformation products of metformin. By employing the isoconversional methods, the effective activation energies were found to vary with the reaction temperatures in the range of 200−300 kJ/mol according to the Friedman isoconversional method. This variation can be explained by multi-step mechanisms,

The variation of E_α with the extent of conversion in the decomposition region was explained based on the outcomes of our recent study [25], where different decomposition pathways of metformin were discussed. As for the oxidation mechanism, we presented different scenarios for O_2(t) and O(t) attacks on metformin, which can explain the variation of the E_α in our experiments. The experimental E_α value for the oxidation mechanism ranges between 280 and 420 kJ/mol, which lies within the calculated activation barriers of the O_2(t) attacks on metformin, indicating that the oxidation is ruled by molecular rather than atomic oxygen attacks.

Using the isoconversional method of Friedman, the kinetic triplet, A, $\Delta S^{\ddagger}$, and $\Delta G^{\ddagger}$ were also determined. This was done by finding the appropriate reaction model $f(\alpha)$. which was best fitted to a three-dimensional diffusion function. The A values were found to vary with the extent of conversion, in agreement with the trend of E_α. The activation entropies ($\Delta S^{\ddagger}$) in the middle temperature region were found to be positive, incomplete support to the nature of thermal decomposition, where disorder increases in the transition state.

The outcomes of this research enrich our understanding of the thermo-oxidative decomposition of pharmaceutical compounds, and shape a benchmark for any future implementation of the catalytic conversion of nitrogen-rich water contaminates as a source of carbon-free fuel or value-added products.

CRediT authorship contribution statement

Ismail Badran: Conceptualization, Writing - original draft. **Abdallah D. Manasrah:** Methodology, Visualization, Validation, Writing - original draft. **Azfar Hassan:** Methodology, Data curation, Validation. **Nashaat N. Nassar:** Conceptualization, Supervision, Funding acquisition, Project administration, Writing - review & editing.

Declaration of Competing Interest

The authors declare that there is no conflict of interest regarding the publication of this article

Acknowledgements

The authors are grateful to the College of Arts and Sciences at Qatar University, the Natural Sciences and Engineering Research Council of Canada (NSERC), the Department of Chemical and Petroleum Engineeringat the Schulich School of Engineering at the University of Calgary. This research was enabled in part by support provided by Compute Canada.

Appendix A. Supplementary data

Supplementary material related to this article can be found, in the online version, at doi:https://doi.org/10.1016/j.tca.2020.178797.

References

[1] I. Rodea-Palomares, M. Gonzalez-Pleiter, S. Gonzalo, R. Rosal, F. Leganes, S. Sabater, M. Casellas, R. Muñoz-Carpena, F. Fernández-Piñas, Hidden drivers of low-dose pharmaceutical pollutant mixtures revealed by the novel GSA-QHTS screening method, Sci. Adv. 2 (9) (2016), e1601272, https://doi.org/10.1126/sciadv.1601272.

[2] A. Kot-Wasik, A. Jakimska, M. Śliwka-Kaszyńska, Occurrence and seasonal variations of 25 pharmaceutical residues in wastewater and drinking water treatment plants, Environ. Monit. Assess. 188 (12) (2016) 661, https://doi.org/10.1007/s10661-016-5637-0.

[3] C. Gadipelly, A. Pérez-González, G.D. Yadav, I. Ortiz, R. Ibáñez, V.K. Rathod, K. V. Marathe, Pharmaceutical industry wastewater: review of the technologies for water treatment and reuse, Ind. Eng. Chem. Res. 53 (29) (2014) 11571–11592.

[4] Y. Luo, W. Guo, H.H. Ngo, L.D. Nghiem, F.I. Hai, J. Zhang, S. Liang, X.C. Wang, A review on the occurrence of micropollutants in the aquatic environment and their fate and removal during wastewater treatment, Sci. Total Environ. 473-474 (2014) 619–641, https://doi.org/10.1016/j.scitotenv.2013.12.065.

[5] P.M. Bradley, C.A. Journey, D.T. Button, D.M. Carlisle, J.M. Clark, B.J. Mahler, N. Nakagaki, S.L. Qi, I.R. Waite, P.C. VanMetre, Metformin and other pharmaceuticals widespread in wadeable streams of the southeastern United States, Environ. Sci. Technol. Lett. 3 (6) (2016) 243–249, https://doi.org/10.1021/acs.estlett.6b00170.

[6] M. Alnajjar, A. Hethnawi, G. Nafie, A. Hassan, G. Vitale, N.N. Nassar, Silica-alumina composite as an effective adsorbent for the removal of metformin from water, J. Environ. Chem. Eng. 7 (3) (2019), 102994, https://doi.org/10.1016/j.jece.2019.102994.

[7] R.M. Briones, A.K. Sarmah, L.P. Padhye, A global perspective on the use, occurrence, fate and effects of anti-diabetic drug metformin in natural and engineered ecosystems, Environ. Pollut. 219 (2016) 1007–1020, https://doi.org/10.1016/j.envpol.2016.07.040.

[8] S. Zhu, Y.-g Liu, S.-b Liu, G.-m Zeng, L.-h Jiang, X.-f Tan, L. Zhou, W. Zeng, T.-t Li, C.-p. Yang, Adsorption of emerging contaminant metformin using graphene oxide, Chemosphere 179 (2017) 20–28, https://doi.org/10.1016/j.chemosphere.2017.03.071.

[9] N.J. Niemuth, R. Jordan, J. Crago, C. Blanksma, R. Johnson, R.D. Klaper, Metformin exposure at environmentally relevant concentrations causes potential endocrine disruption in adult male fish, Environ. Toxicol. Chem. 34 (2) (2015) 291–296, https://doi.org/10.1002/etc.2793.

[10] M. Scheurer, A. Michel, H.-J. Brauch, W. Ruck, F. Sacher, Occurrence and fate of the antidiabetic drug metformin and its metabolite guanylurea in the environment and during drinking water treatment, Water Res. 46 (15) (2012) 4790–4802.

[11] X. Sui, Y. Xu, X. Wang, W. Han, H. Pan, M. Xiao, Metformin: a novel but controversial drug in cancer prevention and treatment, Mol. Pharm. 12 (11) (2015) 3783–3791, https://doi.org/10.1021/acs.molpharmaceut.5b00577.

[12] C. Coyle, F.H. Cafferty, C. Vale, R.E. Langley, Metformin as an adjuvant treatment for cancer: a systematic review and meta-analysis, Ann. Oncol. 27 (12) (2016) 2184–2195, https://doi.org/10.1093/annonc/mdw410.

[13] Y. Lei, Y. Yi, Y. Liu, X. Liu, E.T. Keller, C.-N. Qian, J. Zhang, Y. Lu, Metformin targets multiple signaling pathways in cancer, Chin. J. Cancer 36 (1) (2017) 17, https://doi.org/10.1186/s40880-017-0184-9.

[14] S. Tisler, C. Zwiener, Formation and occurrence of transformation products of metformin in wastewater and surface water, Sci. Total Environ. 628-629 (2018) 1121–1129, https://doi.org/10.1016/j.scitotenv.2018.02.105.

[15] U.S. Food, Drug Administration, FDA Updates and Press Announcements on NDMA in Metformin, 2020.

[16] I. Badran, A.D. Manasrah, N. Nassar Nashaat, A combined experimental and density functional theory study of metformin oxy-cracking for pharmaceutical wastewater treatment, RSC Adv. 9 (24) (2019) 13403–13413, https://doi.org/10.1039/C9RA01641D.

[17] R.D. MacLaren, K. Wisniewski, C. MacLaren, Environmental concentrations of metformin exposure affect aggressive behavior in the Siamese fighting fish, Betta splendens, PLoS One 13 (5) (2018), https://doi.org/10.1371/journal.pone.0197259.

[18] M. Łach, J. Mikuła, M. Hebda, Thermal analysis of the by-products of waste combustion, J. Therm. Anal. Calorim. 125 (3) (2016) 1035–1045, https://doi.org/10.1007/s10973-016-5512-9.

[19] T. Tong, M. Elimelech, The global rise of zero liquid discharge for wastewater management: drivers, technologies, and future directions, Environ. Sci. Technol. 50 (13) (2016) 6846–6855, https://doi.org/10.1021/acs.est.6b01000.

[20] L.F. Cusioli, H.B. Quesada, A.L. de Brito Portela Castro, R.G. Gomes, R. Bergamasco, Development of a new low-cost adsorbent functionalized with iron nanoparticles for removal of metformin from contaminated water, Chemosphere 247 (2020), 125852, https://doi.org/10.1016/j.chemosphere.2020.125852.

[21] A. Hethnawi, M. Alnajjar, A.D. Manasrah, A. Hassan, G. Vitale, R. Jeong, N. N. Nassar, Metformin removal from water using fixed-bed column of Silica-Alumina composite, Colloids Surf. A Physicochem. Eng. Asp. (2020), 124814, https://doi.org/10.1016/j.colsurfa.2020.124814.

[22] A. El-Qanni, N.N. Nassar, G. Vitale, A. Hassan, Maghemite nanosorbcats for methylene blue adsorption and subsequent catalytic thermo-oxidative decomposition: computational modeling and thermodynamics studies, J. Colloid Interface Sci. 461 (2016) 396–408, https://doi.org/10.1016/j.jcis.2015.09.041.

[23] A. El-Qanni, N.N. Nassar, G. Vitale, A combined experimental and computational modeling study on adsorption of propionic acid onto silica-embedded NiO/MgO nanoparticles, Chem. Eng. J. 327 (2017) 666–677, https://doi.org/10.1016/j.cej.2017.06.126.

[24] I. Badran, R. Khalaf, Adsorptive removal of alizarin dye from wastewater using maghemite nanoadsorbents, Sep. Sci. Technol. (2019) 1–16, https://doi.org/10.1080/01496395.2019.1634731.

[25] I. Badran, A. Hassan, A.D. Manasrah, N.N. Nassar, Experimental and theoretical studies on the thermal decomposition of metformin, J. Therm. Anal. Calorim. 138 (1) (2019) 433–441, https://doi.org/10.1007/s10973-019-08213-9.

[26] M.A. Mohamed, A.K. Attia, Thermal behavior and decomposition kinetics of cinnarizine under isothermal and non-isothermal conditions, J. Therm. Anal. Calorim. 127 (2) (2017) 1751–1756, https://doi.org/10.1007/s10973-016-5551-2.

[27] V.L. Stanford, S. Vyazovkin, Thermal decomposition kinetics of malonic acid in the condensed phase, Ind. Eng. Chem. Res. 56 (28) (2017) 7964–7970, https://doi.org/10.1021/acs.iecr.7b02076.

[28] J.D. Menczel, R.B. Prime, Thermal Analysis of Polymers : Fundamentals and Applications, John Wiley, Hoboken, N.J. USA, 2009.

[29] S. Vyazovkin, Isoconversional Kinetics of Thermally Stimulated Processes, Springer, New York, NY, USA, 2015.

[30] OriginLab Corporation, OriginPro 9.1: Scientific Data Analysis and Graphing Software, OriginLab Corporation, Northampton, MA, USA, 2019.

[31] I. Badran, A. Rauk, Y. Shi, New orbital symmetry-allowed route for cycloreversion of Silacyclobutane and its methyl derivatives, J. Phys. Chem. A 123 (9) (2019) 1749–1757, https://doi.org/10.1021/acs.jpca.8b08071.

[32] A.D. Becke, Density-functional thermochemistry. III. The role of exact exchange, J. Chem. Phys. 98 (7) (1993) 5648–5652.

[33] A.P. Scott, L. Radom, Harmonic vibrational frequencies: an evaluation of hartree−Fock, møller−Plesset, quadratic configuration interaction, density functional theory, and semiempirical scale factors, J. Phys. Chem. 100 (41) (1996) 16502–16513, https://doi.org/10.1021/jp960976r.

[34] M. Head-Gordon, J.A. Pople, M.J. Frisch, MP2 energy evaluation by direct methods, Chem. Phys. Lett. 153 (6) (1988) 503–506.

[35] J.S. Binkley, J.A. Pople, Møller–Plesset theory for atomic ground state energies, Int. J. Quantum Chem. 9 (2) (1975) 229–236, https://doi.org/10.1002/qua.560090204.

[36] M. Frisch, G. Trucks, H. Schlegel, G. Scuseria, M. Robb, J. Cheeseman, G. Scalmani, V. Barone, G. Petersson, H. Nakatsuji, Gaussian 16, Revision A. 03, Gaussian Inc, Wallingford CT, 2016.

[37] R. Dennington, T. Keith, J. Millam, GaussView, Version 5, 2009.

[38] Sigma-Aldrich Metformin, Catalogue Number PHR1084 Sigma-aldrich Corporation, 2018. www.sigmaaldrichchem.com.

[39] S. Vyazovkin, A.K. Burnham, J.M. Criado, L.A. Pérez-Maqueda, C. Popescu, N. Sbirrazzuoli, ICTAC Kinetics Committee recommendations for performing kinetic computations on thermal analysis data, Thermochim. Acta 520 (1) (2011) 1–19, https://doi.org/10.1016/j.tca.2011.03.034.

[40] S. Vyazovkin, A.K. Burnham, J.M. Criado, L.A. Pérez-Maqueda, C. Popescu, N. Sbirrazzuoli, ICTAC Kinetics Committee recommendations for performing kinetic computations on thermal analysis data, Thermochim. Acta 520 (1–2) (2011) 1–19, https://doi.org/10.1016/j.tca.2011.03.034.

[41] H.L. Friedman, New methods for evaluating kinetic parameters from thermal analysis data, J. Polym. Sci. B 7 (1) (1969) 41–46, https://doi.org/10.1002/pol.1969.110070109.

[42] H.E. Kissinger, Reaction kinetics in differential thermal analysis, Anal. Chem. 29 (11) (1957) 1702–1706, https://doi.org/10.1021/ac60131a045.

[43] T. Akahira, T. Sunose, Method of determining activation deterioration constant of electrical insulating materials, Res. Rep. Chiba Inst. Technol. (Sci. Technol.) 16 (1971) (1971) 22–31.

[44] S. Vyazovkin, C.A. Wight, Isothermal and non-isothermal kinetics of thermally stimulated reactions of solids, Int. Rev. Phys. Chem. 17 (3) (1998) 407–433, https://doi.org/10.1080/014423598230108.

[45] N.N. Nassar, A. Hassan, G. Vitale, Comparing kinetics and mechanism of adsorption and thermo-oxidative decomposition of Athabasca asphaltenes onto TiO2, ZrO2, and CeO2 nanoparticles, Appl. Catal. A Gen. 484 (2014) 161–171, https://doi.org/10.1016/j.apcata.2014.07.017.

[46] I. Badran, N.N. Nassar, N.N. Marei, A. Hassan, Theoretical and thermogravimetric study on the thermo-oxidative decomposition of Quinolin-65 as an asphaltene model molecule, RSC Adv. 6 (59) (2016) 54418–54430, https://doi.org/10.1039/C6RA07761G.

[47] Y.-R. Luo, Comprehensive Handbook of Chemical Bond Energies, CRC press, Boca Raton, Florida, USA, 2007.

[48] Y. Hao, J. Peng, S. Hu, J. Li, M. Zhai, Thermal decomposition of allyl-imidazolium-based ionic liquid studied by TGA–MS analysis and DFT calculations, Thermochim. Acta 501 (1) (2010) 78–83, https://doi.org/10.1016/j.tca.2010.01.013.

[49] C. Dong, X. Song, J. Zhang, D. Liu, E.J. Meijer, J. Yu, Thermodynamics and kinetics analysis of thermal dissociation of tri-n-octylamine hydrochloride in open system: a DFT and TGA study, Thermochim. Acta 670 (2018) 35–43, https://doi.org/10.1016/j.tca.2018.05.017.

[50] P.W. Atkins, J. De Paula, J. Keeler, Atkins' Physical Chemistry, 11th ed., Oxford University Press, Oxford, United Kingdom; New York, NY, 2018.

[51] I. Badran, Hot-wire Chemical Vapour Deposition Chemistry and Kinetics of New Precursors in the Gas Phase and on the Wire Surface [PhD], University of Calgary, Calgary, Alberta, Canada, 2014.
[52] C.A. Taatjes, D.L. Osborn, T.M. Selby, G. Meloni, A.J. Trevitt, E. Epifanovsky, A. I. Krylov, B. Sirjean, E. Dames, H. Wang, Products of the benzene+ O (3P) reaction, J. Phys. Chem. A 114 (9) (2010) 3355–3370, https://doi.org/10.1021/jp9114145.
[53] X. Song, M.G. Fanelli, J.M. Cook, F. Bai, C.A. Parish, Mechanisms for the reaction of thiophene and methylthiophene with singlet and triplet molecular oxygen, J. Phys. Chem. A 116 (20) (2012) 4934–4946, https://doi.org/10.1021/jp301919g.
[54] J.A. Miller, M.J. Pilling, J. Troe, Unravelling combustion mechanisms through a quantitative understanding of elementary reactions, Proc. Combust. Inst. 30 (1) (2005) 43–88.
[55] A.S. Sharipov, A.M. Starik, Theoretical study of the reaction of ethane with oxygen molecules in the ground triplet and Singlet Delta states, J. Phys. Chem. A 116 (33) (2012) 8444–8454, https://doi.org/10.1021/jp304906u.
[56] S. Asgharzade, M. Vahedpour, Mechanism and rate constants for ammonia photochemical oxidation with O2 on the singlet and triplet potential energy surfaces, Struct. Chem. 25 (4) (2014) 1057–1065, https://doi.org/10.1007/s11224-013-0375-1.
[57] A.D. Manasrah, A. El-Qanni, I. Badran, L.C. Ortega, M.J. Perez-Zurita, N.N. Nassar, Experimental and theoretical studies on oxy-cracking of Quinolin-65 as a model molecule for residual feedstocks, React. Chem. Eng. 2 (5) (2017) 703–719, https://doi.org/10.1039/c7re00048k.
[58] W.M. Haynes, CRC Handbook of Chemistry and Physics, CRC press, Boca Raton, Florida, USA, 2014.
[59] T. Engel, P. Reid, T. Engel, W. Hehre, Physical Chemistry, 3rd ed., Pearson, Boston, 2013.
[60] N. Sbirrazzuoli, Y. Girault, L. Elégant, Simulations for evaluation of kinetic methods in differential scanning calorimetry. Part 3 — peak maximum evolution methods and isoconversional methods, Thermochim. Acta 293 (1997) 25–37, https://doi.org/10.1016/S0040-6031(97)00023-3.
[61] N. Sbirrazzuoli, Determination of pre-exponential factors and of the mathematical functions f(α) or G(α) that describe the reaction mechanism in a model-free way, Thermochim. Acta 564 (2013) 59–69, https://doi.org/10.1016/j.tca.2013.04.015.
[62] N. Sbirrazzuoli, Determination of pre-exponential factor and reaction mechanism in a model-free way, Thermochim. Acta 691 (2020), 178707, https://doi.org/10.1016/j.tca.2020.178707.